crystals

MDPI

Article

Density Functional Theory Study of Lanthanide Monoxides under High Pressure: Pressure-Induced B1–B2 Transition

Sergio Ferrari [1,2] and Daniel Errandonea [3,*]

[1] Departamento Física Experimental, CNEA, Centro Atómico Constituyentes, Av. Gral. Paz 1499, San Martín 1650, Argentina; sergioferrari@cnea.gob.ar
[2] Consejo Nacional de Ciencia y Tecnología, Ciudad Autónoma de Buenos Aires 1650, Argentina
[3] Departamento de Física Aplicada-ICMUV, MALTA Consolider Team, Universidad de Valencia, Dr. Moliner 50, Burjassot, 46100 Valencia, Spain
* Correspondence: daniel.errandonea@uv.es

Abstract: Using density functional theory, we study the influence of hydrostatic pressure on the crystal structure of lanthanide monoxides, focusing on the monoxides formed by the fifteen elements of the lanthanide series, from La to Lu. Calculations are performed using two methods for the ambient pressure B1 (NaCl type) structure, the general gradient approximation (GGA) and the local density approximation (LDA). Through a systematic comparison with existent experimental data, we find that the first method agrees better with the experiments. In addition, considering other cubic structures previously reported for lanthanide monoxides, as B2 (CsCl type) and B3 (ZnS type), we explore the possibility of the occurrence of pressure-induced phase transitions. Based on the better accuracy of GGA to describe the B1 phase at ambient conditions, we exclusively use GGA for the high pressure study. We find, for the fifteen studied compounds, that, at ambient pressure, the B1 structure is the one with the lowest enthalpy, being therefore the most thermodynamically stable structure. We also determine that, at elevated pressures, all the studied compounds undergo a structural phase transition to the B2 phase. We finally establish the relationship between pressure and volume of the unit cell, along with the associated isothermal equation of state, determining the bulk modulus.

Keywords: lanthanide monoxide; high pressure; phase transition; density functional theory

check for updates

Citation: Ferrari, S.; Errandonea, D. Density Functional Theory Study of Lanthanide Monoxides under High Pressure: Pressure-Induced B1–B2 Transition. *Crystals* **2024**, *14*, 831. https://doi.org/10.3390/cryst14100831

Academic Editor: Weiqiang Lv

Received: 5 September 2024
Revised: 19 September 2024
Accepted: 21 September 2024
Published: 25 September 2024

Copyright: © 2024 by the authors. Licensee MDPI, Basel, Switzerland. This article is an open access article distributed under the terms and conditions of the Creative Commons Attribution (CC BY) license (https://creativecommons.org/licenses/by/4.0/).

1. Introduction

Divalent lanthanide monoxides have been known to exist since the 1970s or possibly even earlier [1–3]. However, due to the challenges faced when synthesizing them and their weak chemical stability, their solid forms have not been studied until recently [4–9], after being successfully grown as thin films. Despite recent efforts, very little is known about their crystal structure, and nothing is known about their structural behavior under high-pressure conditions. For instance, are they stable under high hydrostatic pressure? The crystal structure, structural stability, and elastic parameters like the bulk modulus are fundamental descriptors of solids and a necessary input for accurately characterizing other physical properties. Therefore, it is timely to perform a study on lanthanide monoxides under high-pressure conditions.

Part of the recent interest in lanthanide monoxides comes from their magnetic properties at low temperatures [6]. For instance, lanthanum monoxide, LaO, has been reported to be a ferromagnetic semiconductor with a narrow band gap of 0.11 eV and a Curie temperature of 130 K. Furthermore, the intense search of high-temperature superconductivity using high pressure [10] includes also compounds such us LaO [11]. This compound has been reported to exhibit a stronger superconductivity compared to lanthanide monochalcogenides, with a critical temperature of approximately 5 K [11]. The normal state of superconducting LaO has been proposed to be a $\mathbb{Z}_2$ nontrivial topological metal, where the Dirac point protected by the crystal symmetry is located around the Fermi energy [12], rendering LaO

a rather interesting system. The superconducting properties of LaO and other lanthanide monoxides, such as SmO [13], which is classified as a heavy-fermion compound, can be adjusted to increase the critical temperature by applying an external pressure [14]. Hydrostatic pressure reduces the unit-cell volume and, as a result, the interatomic distances and, consequently, physical interactions, including the electron–phonon coupling [14]. Thus, a characterization of the influence of hydrostatic pressure on the crystal structure is fundamental for improving understanding of high-pressure superconductivity [15].

Beyond the superconducting properties, lanthanide monoxides have also attracted broad interest due to their potential applications in various fields, including chemistry, biology, medicine, and the high-technology industry [16]. In addition, monoxides of lanthanides are of special interest because of their variable stoichiometry and diverse electrical and magnetic properties [17]. Another reason for the growing interest in lanthanide monoxides is that these materials can be used as models to simulate the properties of the monoxides of the transuranic elements, including plutonium monoxide, a waste form of plutonium conversion. The study of the monoxides of the transuranic elements has been gaining considerable attention to improve the safety of storing nuclear waste [18]. However, they are more difficult to study than lanthanide monoxides due the radioactivity of transuranic elements.

With the aim of contributing to improving the understanding of lanthanide monoxides, we perform a systematic computational study considering the monoxides of fifteen lanthanides (from La to Lu). The study of the whole series is important for developing a systematic understanding of the structural properties and high-pressure behavior of lanthanide monoxides. Calculations are performed at ambient pressure and under high pressure using the density functional theory and the Quantum Espresso open-source package [19]. We perform calculations under the general gradient approximation (GGA) [20] and the local density approximation (LDA) [21] to check the accuracy of both functionals to describe lanthanide monoxides. For the modeling of the crystal structure of the studied compounds, we evaluate three candidate structures, the cubic B1 (NaCl type), B2 (CsCl type), and B3 (ZnS type) structures, all of which have been reported in the past as possible structures for lanthanide monoxides [3,6,22,23]. By comparing our results with previous experiments, we find that GGA is the approximation that best describes lanthanide monoxides. By means of total energy and enthalpy calculations, we also find that, for the fifteen studied compounds, the most thermodynamically stable structure is B1. However, we also conclude that all the studied lanthanide monoxides are expected to undergo a B1–B2 phase transition under high-pressure conditions. The change of the unit-cell volume for all compounds is also calculated. From these results, an isothermal equation of state (EOS) is obtained for each compound. The results are systematically discussed.

2. Materials and Methods

To investigate the structural properties of lanthanide monoxides and the phase transitions induced by pressure on them, we conducted ab initio calculations at zero temperature using the density functional theory [24,25] with the pseudopotentials and plane-wave method (PP–PW), as implemented in the Quantum Espresso (QE) code. In this approach, the ionic cores were represented using ultrasoft pseudopotentials from the standard solid state pseudopotentials library (SSSP) [26]. This approximation makes DFT calculations less computationally expensive, as only valence electrons are treated explicitly. Based on convergence tests, we established a kinetic energy cutoff of 85 Ry for the plane waves and a cutoff of 1190 Ry for the charge density and potential. These values ensured reliable results across all computations. The traditional Monkhorst–Pack scheme [27] was employed by using a dense grid of $10 \times 10 \times 10$ to sample the Brillouin zone. In our total energy calculations, we used the generalized gradient approximation (GGA) and the local density approximation (LDA) for the exchange–correlation (XC) energy for the case of the B1 phase. We employed the Ceperley–Alder expression for the LDA XC functional and the expression introduced by Perdew, Burke, and Ernzerhof (PBE) for the GGA XC functional. Since we found that

the first method gives more accurate results for the ambient pressure structure, to study the structural stability under pressure of the studied compounds, only GGA was used. For the study under high-pressure conditions, the different crystal structures were optimized at fixed volumes. The pressure (P) was derived from the energy (E) versus volume (V) graphs by calculating the derivative of the total energy in relation to volume. The enthalpy (H) was then obtained for each structure as H = E + P × V. Since calculations were performed at 0 K temperature, there was no need in this study to calculate the vibrational frequencies and entropy under different pressures to compare the Gibbs energies of different phases as a function of pressure. This approximation has provided accurate results for the study of compounds crystallizing in the B1 structure under high-pressure conditions [28], and is normally used for the prediction of phase transitions in oxides under compression [29,30].

During the generation of pseudopotentials, all but one of the *f* electrons for the lanthanide atoms were frozen into the core, while, with regard to oxygen atoms, the $2s^2$ and $2p^4$ electrons were explicitly treated as valence electrons. For each studied monoxide, we calculated the energy across various lattice constants and corresponding volumes to determine the equilibrium properties of their cubic structures. The energy–volume results were fitted using the Birch–Murnaghan equation of state [31], yielding the equilibrium volume, equilibrium energy, bulk modulus, and the pressure derivative of the bulk modulus for each structure. Additionally, we computed the enthalpy as a function of pressure to explore both the possible occurrence of structural phase transitions and the transition pressures. To explore the high-pressure stability, we focused on the three cubic phases referred to as stable or metastable phases in the literature [3,6,22,23]: B1 (NaCl type), B2 (CsCl type), and B3 (ZnS type), all of which are shown in Figure 1. The B1 structure is described by space group $Fm\bar{3}m$, with the lanthanide atoms at the 4a Wyckoff position (0,0,0) and the oxygen atoms at the 4b Wyckoff position (1/2,1/2,1/2). The B2 structure is described by space group $Pm\bar{3}m$, with the lanthanide atoms at the 1a Wyckoff position (0,0,0) and the oxygen atoms at the 1b Wyckoff position (1/2,1/2,1/2). The B3 structure is described by space group $F\bar{4}3m$, with the lanthanide atoms at the 4a Wyckoff position (0,0,0) and the oxygen atoms at the 4c Wyckoff position (1/4,1/4,1/4).

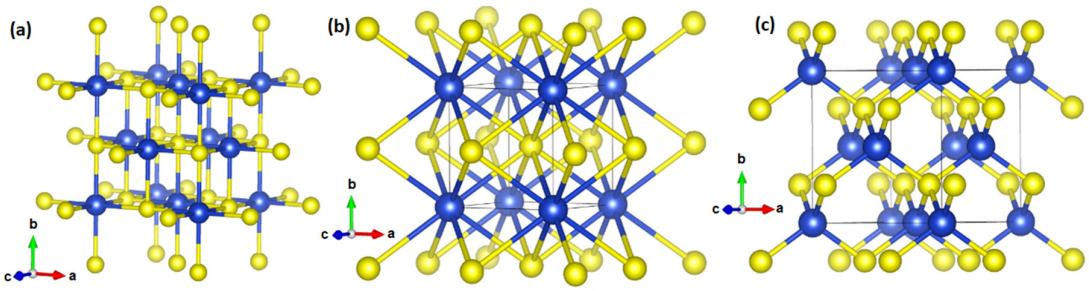

Figure 1. Crystal structure of the (**a**) B1, (**b**) B2, and (**c**) B3 phases. The blue (yellow) spheres represent the lanthanide (oxygen) atoms.

3. Results and Discussion

Figures 2–5 show the calculated enthalpy versus pressure for the fifteen studied compounds using the GGA approximation. In all the figures, it can the seen that, at 0 GPa, the B1 structure was the one with the lowest enthalpy, indicating that, at ambient pressure, B1 is the most thermodynamically stable structure among the fifteen studied compounds. This result agrees with the fact that most experiments performed on lanthanide monoxides have reported that they have the B1 structure.

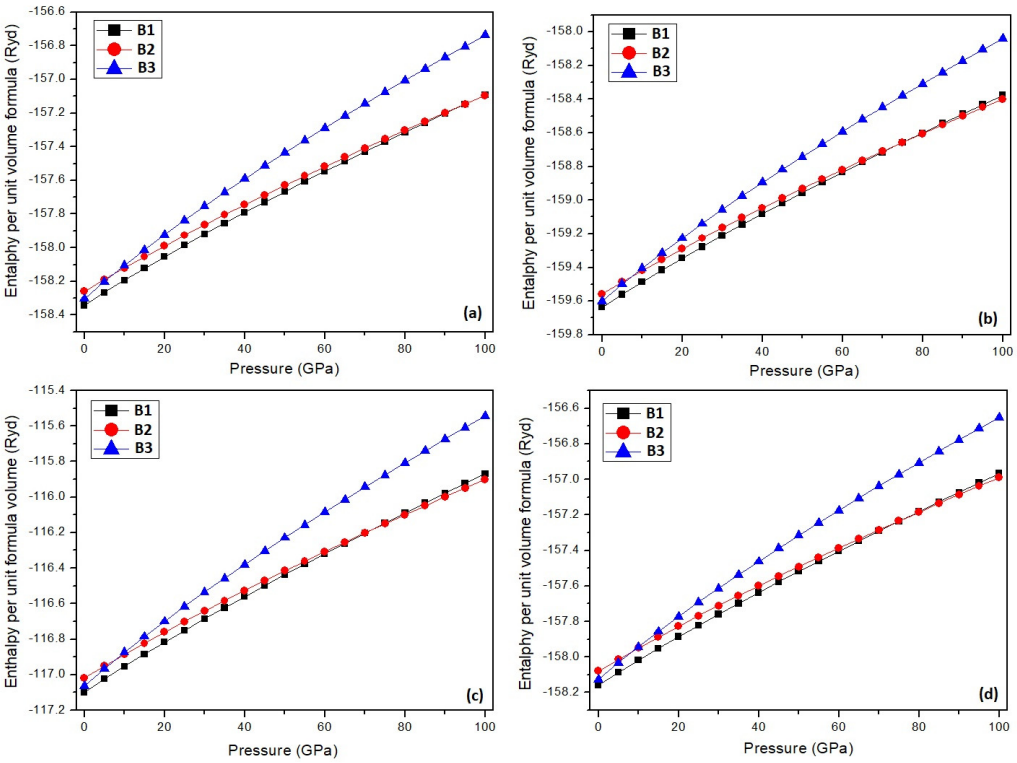

Figure 2. Enthalpy versus pressure for the three phases considered for (**a**) LaO, (**b**) CeO, (**c**) PrO, and (**d**) NdO.

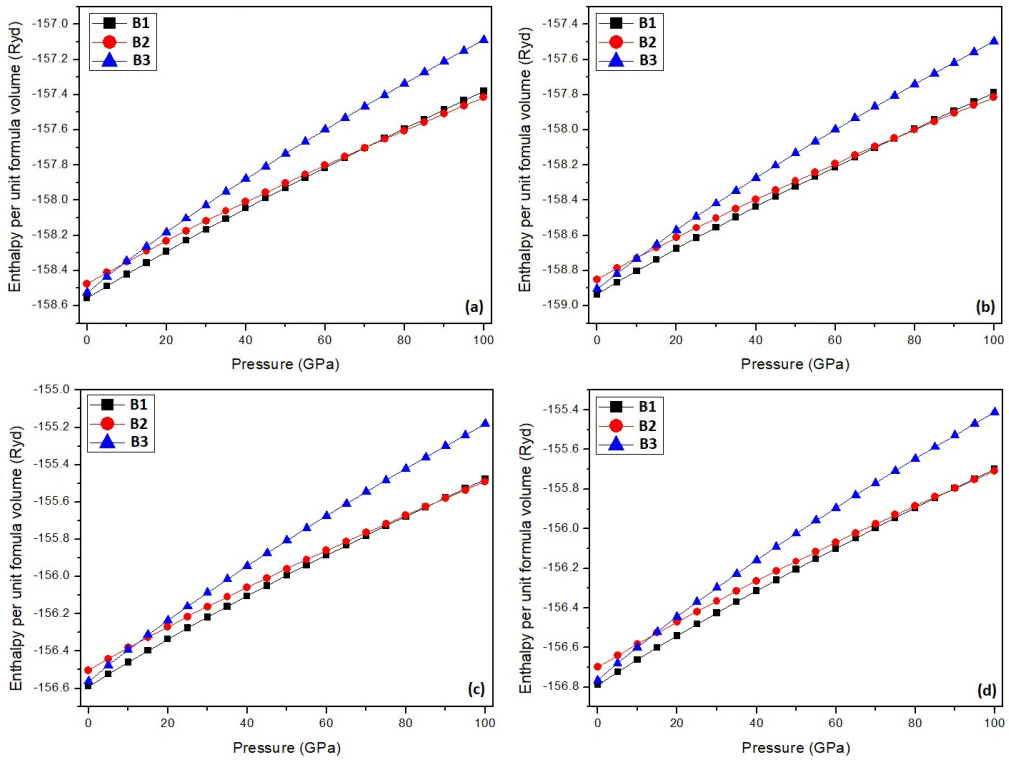

Figure 3. Enthalpy versus pressure for the three phases considered for (**a**) PmO, (**b**) SmO, (**c**) EuO, and (**d**) GdO.

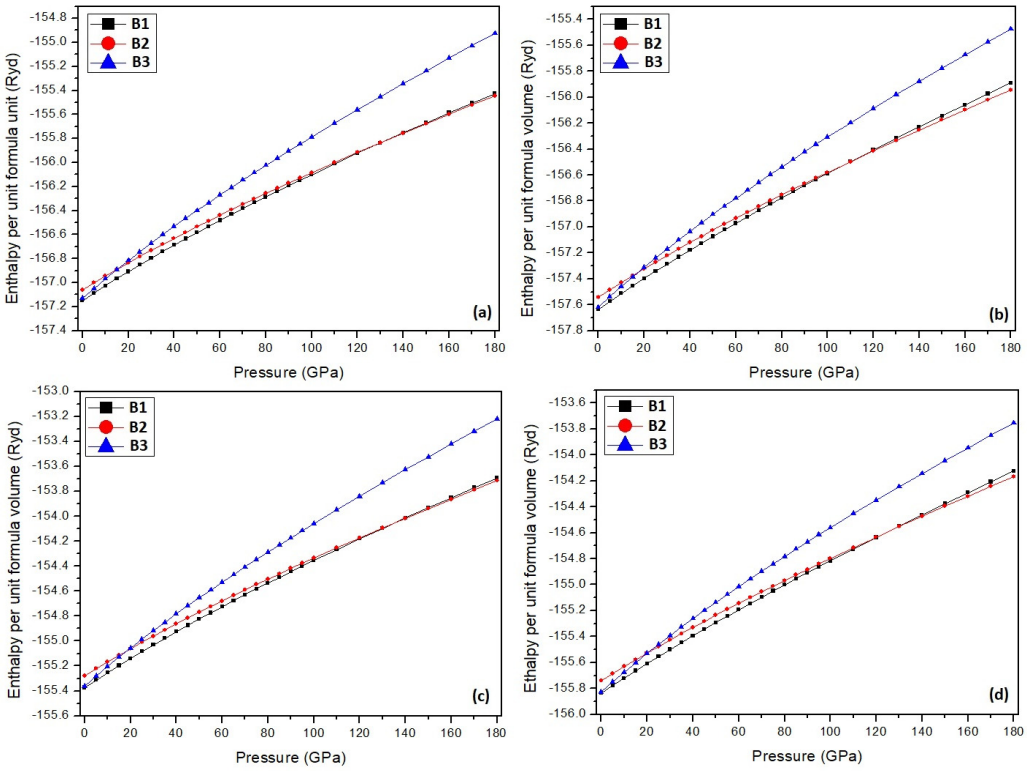

Figure 4. Enthalpy versus pressure for the three phases considered for (**a**) TbO, (**b**) DyO, (**c**) HoO, and (**d**) ErO.

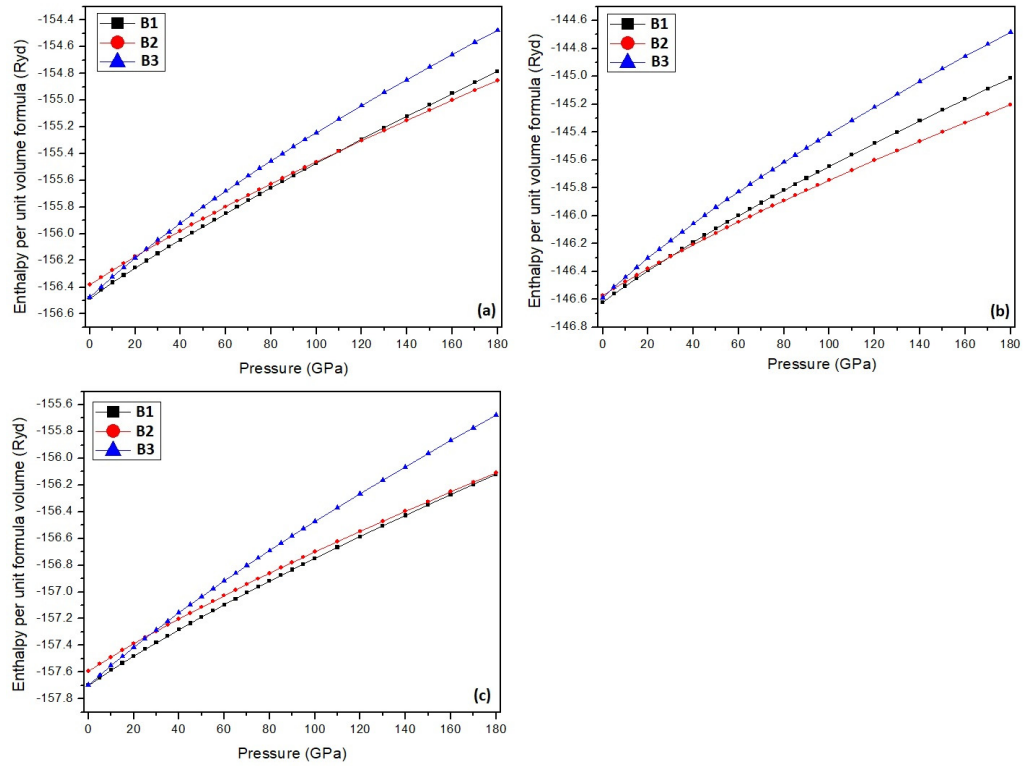

Figure 5. Enthalpy versus pressure for the three phases considered for (**a**) TmO, (**b**) YbO, and (**c**) LuO.

Interestingly, at 0 GPa, the structure closest in enthalpy to B1 was B3, a phenomenon which is consistent with the fact that it has been observed as a metastable phase in com-

pounds like GdO, SmO, and EuO [3,23]. For compounds already experimentally reported, the unit-cell parameters calculated in this work are summarized in Table 1. In the table, we include results from GGA and LDA calculations and from previous experiments [13,32,32–45]. In Table 2, we summarize the results we obtained for the fifteen studied compounds, including those never studied experimentally, for the interest of future studies.

Table 1. Experimental and calculated unit-cell constant (in Å) of experimentally reported lanthanide monoxides in the B1 phase. The references from which the experimental results were extracted are indicated in the table. The average of the experimental values is also shown, with the standard deviation between brackets. Results from Ref. [5] are also reported for comparison.

	Experiments	Average of Experimental Values	QE Calculations GGA This Work	QE Calculations LDA This Work	WIEN2k Calculations GGA, Ref. [5]
LaO	5.144 [32] 5.125 [33] 5.198 [14]	5.156 (4)	5.1643	5.0583	5.1102
CeO	5.089 [32] 5.089 [32]	5.089 (1)	5.1312	5.0244	4.9931
PrO	5.031 [32] 5.031 [32] 5.0316 [34]	5.0312 (3)	5.0677	4.9600	4.9295
NdO	4.994 [32] 4.9960 [32] 5.0101 [35]	5.000 (8)	5.0144	4.9051	4.9510
SmO	4.943 [32] 4.9414 [34] 4.9414 [35] 5.015–5.050 [36] 4.9883 [14] 4.94 [37]	4.97 (4)	4.9256	4.8141	4.9592
EuO	5.142 [36] 5.1439 [14] 5.141 [38] 5.1419 [39]	5.1416 (6)	4.8867	4.6103	4.9954
GdO	4.99 [40]	4.99	4.8542	4.73634	
TbO	4.92 [41]	4.92	4.8243	4.58015	4.8009
HoO	4.904 [42]	4.904	4.7629	4.6367	4.7661
YbO	4.877 [43] 4.87 [44] 4.88 [45]	4.876 (5)	4.7205	4.5767	4.6566

Table 1 also shows that GGA agreed better with experiments than LDA, providing a more accurate description of the crystal structure. This result is not surprising, since it is generally accepted that GGA is more accurate than LDA for describing unit-cell parameters. Despite this fact, it is evident that LDA effectively mirrored the trend of the unit-cell parameters observed in GGA calculations and experimental data; however, the values of the unit-cell parameters were comparatively lower. In Table 1, we also compare our results with those from previous computing simulations which were obtained from GGA calculations conducted by Shafiq et al. using the WIEN2k [5]. The table shows that the previous WIEN2k calculations tended to underestimate the value of the lattice parameter, in particular with respect to CeO and PrO. However, they agreed better with experiments than our calculations only with respect to EuO. The differences between our calculations and those performed with WIEN2k [5] might be related to the fact thar WIEN2K is an

all-electron code, not pseudopotential code, or to the use of a different kinetic energy cutoff and a different convergence criterium in calculations.

Table 2. Unit-cell constant (*a*), bulk modulus at zero pressure (B_0), pressure derivative B_0' and pressure of B1–B2 transition of lanthanide monoxides. We also report the relative change in the unit-cell volume per formula unit (ΔV) at the B1–B2 transition. All results were calculated with Quantum Espresso using the GGA method. The bulk moduli from Ref. [5] are included for comparison.

Lanthanide Monoxide	*a* (Å)	B_0 (GPa)	B_0'	B1–B2 Transition Pressure (GPa)	% of ΔV at the B1–B2 Transition	Bulk Modulus Ref. [5] (GPa)
LaO	5.1643	125.1	4.51	96	−0.082	102.663
CeO	5.1312	128.0	4.68	75	−0.076	162.659
PrO	5.0677	133.6	5.17	71	−0.078	146.852
NdO	5.0144	136.9	4.95	77	−0.079	162.557
PmO	4.9673	140.5	6.06	71	−0.078	-
SmO	4.9256	138.5	6.14	77	−0.078	108.327
EuO	4.8867	139.1	5.5	86	−0.077	94.287
GdO	4.8542	137.5	5.63	90	−0.077	-
TbO	4.8243	142.4	3.02	133	−0.077	129.013
DyO	4.7916	148.7	4.84	110	−0.076	-
HoO	4.7629	151.6	3.38	135	−0.075	125.880
ErO	4.7364	149.4	5.64	124	−0.073	106.973
TmO	4.7070	146.6	6.35	111	−0.072	-
YbO	4.7205	124.6	4.44	29	−0.159	226.067
LuO	4.6566	131.1	3.01	209	−0.069	-

On the other hand, the underestimation of the lattice parameter by the LDA method is common in many systems [46] and, apparently, is related to the inherent limitations of LDA in describing the exchange–correlation energy in systems with *f* electrons, like lanthanides. In fact, a similar overestimation of the unit-cell parameter by LDA has been observed with respect to pure lanthanide elements, for which GGA gives also a more accurate description [47]. Based on this fact, the existence of phase transitions under high pressure is discussed using the GGA method.

It should be noted that EuO is the compound for which the largest difference was found between the results of our GGA calculations and experiments. With respect to EuO, the relative difference between both results was 4.8%. This might be related to the fact that Eu^{2+} has the most accessible divalent oxidation state because of the half-filled $4f^7$ electronic configuration of Eu and, consequently, a higher stabilization from exchange energy than other lanthanide elements [47]. This stabilization leads to significant anomalies in the atomic radii of Eu and its physical properties, including the lattice parameter which is the largest among lanthanides [48]. Similar differences to those observed between DFT calculations and experiments for the lattice parameter of EuO have also been reported for europium chalcogenides and pnictides [49]. This phenomenon is a common characteristic of divalent europium compounds and is believed to be associated with an inadequate theoretical representation of f-electron delocalization in europium [50].

We will now discuss the influence of high pressure on the crystal structure of lanthanide monoxides. In Figures 2–5, we show that the difference in enthalpy between phases B1 and B3 increased under compression, making B3 an unsuitable candidate for a high-pressure phase. In contrast, the difference in enthalpy between phases B1 and B2 decreased under compression, leading to phase B2 emerging as the most stable structure once a critical pressure was surpassed. The B1–B2 transition was accompanied by an increase in the coordination number in the first coordination sphere of the lanthanide atoms from six to eight (See Figure 1). The phase transition predicted by our calculations is consistent with the high-pressure characteristics exhibited by other isostructural monoxides such as SrO,

CaO, CdO, and MgO. All these compounds also undergo the B1–B2 transition at 32, 56, 176, and 198 GPa, respectively [51,52].

The transition pressures for the B1–B2 transition in lanthanide monoxides are summarized in Table 2. For most of the studied compounds, they ranged from 71 GPa to 135 GPa. Such pressures can be routinely obtained, nowadays, in laboratories using diamond anvil cells. The only two outliers were YbO, for which a transition pressure of 29 GPa was predicted by our calculations, and LuO, for which a transition pressure of 209 GPa was predicted. Our findings position YbO as the most suitable candidate for the experimental investigation of the B1–B2 transition, as it occurred at a pressure readily accessible with current experimental techniques. Notice that YbO has been synthesized by three different research group; therefore, it would be possible to perform high-pressure x-ray diffraction experiments to test our prediction of the B1–B2 transition. An additional noteworthy finding from Table 2 is that the B1–B2 transition was characterized by a significant volume collapse, a phenomenon that is characteristic of this type of structural transition, which is classified as a reconstructive first-order transition [53]. Summing up, we believe that our findings highlight the importance of leveraging hydrostatic pressure as an additional dimension in the study of lanthanide monoxides, predicting the existence of a B1–B2 transition across all members of this family. Furthermore, they highlight the potential of employing first-principles calculations to plan experiments related to materials that are challenging to synthesize and manipulate.

Additionally, we determined the pressure dependence of the unit-cell volume for phase B1, fitted for each compound using a third-order Birch–Murnaghan equation of state [20]. From the fitting, we obtained the bulk modulus at zero pressure, B_0, and its pressure derivative, B_0'. The bulk modulus is an important mechanical property to determine the substrate influence on the properties of a thin film like those prepared from lanthanide monoxides. The obtained EOS parameters for phase B1 are summarized in Table 2. All compounds showed a bulk modulus between 125 GPa and 152 GPa. Our results imply that lanthanide monoxides are stiffer than CaO, with B_0 = 111 GPa [54], and slightly less stiff than MgO, with B_0 = 156 GPa [55]. Our results show a smooth variation of the bulk modulus when going through the lanthanide series, with the maximum values of the bulk modulus obtained for compounds with a lanthanide atom near the center of the series. The compounds with the smaller bulk modulus were LaO, CeO, YbO, and LuO, while the compounds with the larger bulk modulus were DyO, HoO, and ErO. Our calculations of the bulk modulus contrast with those obtained through elastic constant calculations using the cubic-elastic software [5] and are shown for comparison in Table 2. The difference between both methods for the bulk modulus of LaO was 20%, and the difference was larger for the rest of the compounds compared in Table 2. It should be noted that the bulk moduli obtained from elastic calculations [5] showed an unusual scattering of results with changes in the bulk modulus of up to 120 GPa when moving from one compound to the next one within the family, as it can be seen by comparing the bulk modulus reported for ErO (106.9 GPa) and YbO (226.1 GPa) in Ref. [5]. It is also unreasonable the determination of a bulk modulus of 226 GPa for YbO, as it is more than double the bulk modulus of 94 GPa calculated for EuO using the same method [5]. These unconventional results obtained previously from elastic constant calculations [5] makes us confident in our reported bulk moduli, which follow a smooth behavior when moving from La to Lu along the lanthanide monoxide family. Nevertheless, further high-pressure x-ray diffraction experiments are needed to confirm our results. We hope this work will encourage the research community.

To conclude, for completeness, we present, in Table 3, the unit-cell parameters we obtained for the B2 and B3 phases at 0 GPa, as well as the EOS parameters for the third-order Birch–Murnaghan EOS [31] that describe the pressure dependence of the volume for both phases.

Table 3. Calculated values of the unit-cell constant at zero pressure (*a*), bulk modulus at zero pressure (B0), and its pressure derivative (B_0') for the B2 and B3 structures of the lanthanide monoxides.

Lanthanide Monoxide	*a* B2 Structure (Å)	B_0 B2 Structure (GPa)	B_0' B2 Structure	*a* B3 Structure (Å)	B_0 B3 Structure (GPa)	B_0' B2 Structure
LaO	3.1614	121.0	4.60	5.6698	81.6	3.95
CeO	3.1482	123.3	4.65	5.6300	86.2	4.24
PrO	3.1072	128.0	4.64	5.5624	89.5	4.13
NdO	3.0737	131.7	4.69	5.5053	93.0	4.20
PmO	3.0451	134.3	4.56	5.4553	95.7	4.09
SmO	3.0204	135.7	4.62	5.4103	98.4	4.08
EuO	2.9969	137.4	4.57	5.3667	101.3	4.14
GdO	2.9778	139.5	4.39	5.3290	103.7	4.02
TbO	2.9589	141.9	4.40	5.2920	106.4	4.43
DyO	2.9403	144.7	4.61	5.2565	108.4	4.13
HoO	2.9230	147.6	5.01	5.2229	109.5	4.60
ErO	2.9089	148.1	5.23	5.1948	110.5	4.08
TmO	2.8924	143.2	4.85	5.1623	111.8	3.59
YbO	2.8071	133.0	4.44	5.1267	85.9	4.10
LuO	2.8641	142.6	4.89	5.0996	120.1	4.56

4. Conclusions

In this study, we conduct a comprehensive computational analysis of the structural properties and pressure-induced phase transitions of lanthanide monoxides using the density functional theory with both the generalized gradient approximation (GGA) and the local density approximation (LDA). Our results support that, in the fifteen lanthanide monoxides, the B1 (NaCl type) structure is the most stable phase at ambient pressure for all fifteen studied lanthanide monoxides, a finding which aligns well with previous experimental observations.

Our findings indicate that the GGA method demonstrates greater accuracy in replicating the experimental lattice parameters of the examined compounds at ambient pressure, as opposed to the LDA method which consistently underestimates these parameters. Under high hydrostatic pressure conditions, we predict that all lanthanide monoxides will undergo a phase transition from the B1 to the B2 structure. The transition pressures vary across the series, with YbO showing the lowest transition pressure at 29 GPa, making it an excellent candidate for an experimental verification using current high-pressure techniques. The predicted large volume collapse associated with this phase transition is consistent with the behavior of similar monoxides and underscores the reconstructive nature of the B1–B2 transition. We also calculate the bulk moduli of the fifteen studied compounds, finding that lanthanide monoxides are generally more incompressible than isomorphic CaO but slightly less incompressible than isomorphic MgO. The smooth variation of the values of the bulk modulus through the lanthanide series provides further insights into the material's elastic properties, of relevance for the potential applications of the studied compounds.

In summary, our research contributes to a deeper comprehension of lanthanide monoxides, emphasizing the significance of pressure as a critical factor in their structural analysis. The study provides also structural information and mechanical properties which might be useful for studies on the magnetic and superconducting properties of the material. It also emphasizes the utility of first-principles calculations in guiding future experimental efforts, particularly with respect to the synthesis and high-pressure analysis of these challenging materials we study herein. We hope that our results will stimulate further experimental work to verify the predicted phase transitions and explore the rich physics of lanthanide monoxides under extreme conditions.

Author Contributions: S.F.: investigation; methodology; data curation; writing—review & editing. D.E.: investigation; methodology; data curation; writing—review & editing. All authors have read and agreed to the published version of the manuscript.

Funding: This research was funded with the financial support from the Spanish Ministerio de Ciencia, Innovación y Universidades, MCIU (10.13039/501100011033) under grants RED2022-134388-T and PID2022-138076NB-C41. Daniel Errandonea also acknowledges the financial support obtained from Generalitat Valenciana through the research grants PROMETEO CIPROM/2021/075-GREENMAT and MFA/2022/007. This study forms part of the Advanced Materials Program and is supported by MCIU with funding from the European Union NextGenerationEU fund (PRTR-C17.I1) and by the Generalitat Valenciana.

Data Availability Statement: The data that support the findings of this study are available from the corresponding author upon reasonable request.

Acknowledgments: Sergio Ferrari would like to thank the Comisión Nacional de Energía Atómica (CNEA) from Argentina for hiring him as a scientific researcher and supporting his research.

Conflicts of Interest: The authors declare no conflicts of interest.

References

1. Rauh, E.G.; Ackermann, R.J. The first ionization potentials of neptunium and neptunium monoxide. *J. Chem. Phys.* **1975**, *62*, 1584. [CrossRef]
2. Murad, E.; Hildenbrand, D.L. Dissociation energies of GdO, HoO, ErO, TmO, and LuO; correlation of results for the lanthanide monoxide series. *J. Chem. Phys.* **1980**, *73*, 4005–4011. [CrossRef]
3. Ellinger, F.H.; Zachariasen, W.H. The Crystal Structure of Samarium Metal and of Samarium Monoxide. *J. Amer. Chem. Soc.* **1956**, *76*, 5650–5653.
4. Gan, H.; Zhang, C.; Du, X.Z.; Jiang, P.; Niu, C.P.; Zheng, X.H.; Yin, Y.W.; Li, X.G. Insights into superconductivity of LaO from experiments and first-principles calculations. *Phys. Rev. B* **2021**, *104*, 054515. [CrossRef]
5. Shafiq, M.; Arif, S.; Ahmad, I.; Asadabadi, S.J.; Maqbool, M.; Aliabad, H.A.R. Elastic and mechanical properties of lanthanide monoxides. *J. Alloys Compd.* **2015**, *618*, 292–298. [CrossRef]
6. Kimura, R.; Kaminaga, K.; Kobayashi, T.; Cho, Y.; Maruyama, S.; Maeda, A.; Matsumoto, Y. Elevating the Superconducting Temperature in Epitaxially Stabilized Rock-Salt NbO. *Chem. Mater.* **2024**, *36*, 5028–5036. [CrossRef]
7. Han, Y.; Brugman, B.L.; Leinbach, L.J.; Guo, X.; Leinenweber, K.; Navrotsky, A. Thermochemical properties of high-pressure neodymium monoxide. *Inorg. Chem.* **2024**, *63*, 13468–13473. [CrossRef]
8. Brugman, B.L.; Han, Y.; Leinbach, L.J.; Leinenweber, K.; van de Walle, A.; Ushakov, S.V.; Hong, Q.J.; Navrotsky, A. Computationally led high-pressure synthesis and experimental thermodynamics of Rock Salt yttrium monoxide. *Chem. Mater.* **2024**, *36*, 332–339. [CrossRef]
9. Sano, Y.; Kaminaga, K.; Maruyama, S.; Matsumoto, Y. Ferromagnetic semiconductor EuO thin films characterized by vacuum electrochemical process with ionic liquid. *Mater. Sci. Semicond. Process.* **2024**, *181*, 108629. [CrossRef]
10. Zhong, W.; Zhang, H.; Karaca, E.; Zhou, J.; Kawaguchi, S.; Kadobayashi, H.; Yu, X.; Errandonea, D.; Yue, B.; Hong, F. Pressure-Sensitive Multiple Superconducting Phases and Their Structural Origin in Van der Waals HfS_2 up to 160 GPa. *Phys. Rev. Lett.* **2024**, *133*, 066001. [CrossRef]
11. Sun, P.H.; Zhang, J.F.; Liu, K.; Han, Q.; Lu, Z.Y. First-principles study of the superconductivity in LaO. *Phys. Rev. B* **2021**, *104*, 045121. [CrossRef]
12. Qian, J.; Shen, Z.; Wei, X.; Li, W. $\mathbb{Z}_2$ nontrivial topology of rare-earth binary oxide superconductor LaO. *Phys. Rev. B* **2022**, *105*, L020508. [CrossRef]
13. Uchida, Y.; Kaminaga, K.; Fukumura, T.; Hasegawa, T. Samarium monoxide epitaxial thin film as a possible heavy-fermion compound. *Phys. Rev. B* **2017**, *95*, 125111. [CrossRef]
14. Kaminaga, K.; Oka, D.; Hasegawa, T.; Fukumura, T. Superconductivity of rock-salt structure LaO epitaxial thin film. *J. Am. Chem. Soc.* **2018**, *140*, 6754–6757. [CrossRef]
15. Jurkutat, M.; Kattinger, C.; Tsankov, S.; Haase, J. How pressure enhances the critical temperature of superconductivity in $YBa_2Cu_3O_{6+y}$. *Proc. Natl. Acad. Sci. USA* **2023**, *120*, e22154581. [CrossRef] [PubMed]
16. Chi, C.X.; Xie, H.; Cong, R.; Tang, Z.C.; Zhou, M.F. Electron Affinities of the Early Lanthanide Monoxide Molecules. *Chin. J. Chem. Phys.* **2011**, *24*, 604–610. [CrossRef]
17. Ushakov, S.V.; Hong, Q.-J.; Gilbert, D.A.; Navrotsky, A.; Walle, A.V.D. Thorium and Rare Earth Monoxides and Related Phases. *Materials* **2023**, *16*, 1350. [CrossRef]
18. Harilal, S.S.; Kautz, E.J.; Bernacki, B.E.; Phillips, M.C.; Skrodzki, P.J.; Burger, M.; Jovanovic, I. Physical conditions for UO formation in laser-produced uranium plumes. *Phys. Chem. Chem. Phys.* **2019**, *21*, 16161–16169. [CrossRef]

19. Giannozzi, P.; Baroni, S.; Bonini, N.; Calandra, M.; Car, R.; Cavazzoni, C.; Ceresoli, D.; Chiarotti, G.L.; Cococcioni, M.; Dabo, I.; et al. QUANTUM ESPRESSO: A modular and open-source software project for quantum simulations of materials. *J. Phys. Condens. Matter* **2009**, *21*, 395502. [CrossRef]
20. Perdew, J.P.; Burke, K.; Ernzerhof, M. Generalized gradient approximation made simple. *Phys. Rev. Lett.* **1996**, *77*, 3865. [CrossRef]
21. Sahni, V.; Bohnen, K.P.; Harbola, M.K. Analysis of the local-density approximation of density-functional theory. *Phys. Rev. A* **1988**, *37*, 1895–1907. [CrossRef] [PubMed]
22. Attfiled, J.P.; Ferey, G. Structural correlations within the lanthanum palladium oxide family. *J. Sol. State Chem.* **1989**, *80*, 286–298. [CrossRef]
23. Garg, A.B.; Muñoz, A.; Anzellini, S.; Sanchez-Martín, J.; Turnbull, R.; Díaz-Anichtchenko, D.; Popescu, C.; Errandonea, D. Role of GdO addition in the structural stability of cubic Gd_2O_3 at high pressures: Determination of the equation of states of GdO and Gd_2O_3. *Materialia* **2024**, *34*, 102064. [CrossRef]
24. Hohenberg, P.; Kohn, W. Inhomogeneous Electron Gas. *Phys. Rev.* **1964**, *136*, B864–B871. [CrossRef]
25. Kohn, W.; Sham, L.J. Self-Consistent Equations Including Exchange and Correlation Effects. *Phys. Rev.* **1965**, *140*, A1133–A1138. [CrossRef]
26. Prandini, G.; Marrazzo, A.; Castelli, I.E.; Mounet, N.; Marzari, N. Precision and efficiency in solid-state pseudopotential calculations. *npj Comput. Mater.* **2018**, *4*, 72. [CrossRef]
27. Monkhorst, H.J.; Pack, J.D. Special points for Brillouin-zone integrations. *Phys. Rev. B* **1976**, *13*, 5188–5192. [CrossRef]
28. Recio, J.M.; Flórez, M.; Francisco, E.; Blanco, M.A.; Pendás, A.M. Microscopic Study of the Rock Salt-Caesium Chloride phase stability in alkali halides. *High Press. Res.* **2002**, *22*, 443–446. [CrossRef]
29. Errandonea, D.; Gomis, O.; Santamaría-Perez, D.; García-Domene, B.; Muñoz, A.; Rodríguez-Hernández, P.; Achary, S.N.; Tyagi, A.K.; Popescu, C. Exploring the high-pressure behavior of the three known polymorphs of $BiPO_4$: Discovery of a new polymorph. *J. Appl. Phys.* **2015**, *117*, 105902. [CrossRef]
30. Ouahrani, T.; Muñoz, A.; Franco, R.; Boufatah, R.M.; Bedrane, Z.; Errandonea, D. High-pressure properties of thallium orthovanadate from density-functional theory calculations. *J. Alloys Compd.* **2024**, *978*, 73483. [CrossRef]
31. Birch, F. Finite Elastic Strain of Cubic Crystals. *Phys. Rev.* **1947**, *71*, 809–824. [CrossRef]
32. Leger, J.M.; Yacoubi, N.; Loriers, J. Synthesis of rare earth monoxides. *J. Sol. State Chem.* **1981**, *36*, 261–270. [CrossRef]
33. Griesemer, S.D.; Ward, L.; Wolverton, C. High-throughput crystal structure solution using prototypes. *Phys. Rev. Mater.* **2021**, *5*, 105003. [CrossRef]
34. Krill, G.; Ravet, M.F.; Kappler, J.P.; Abadli, L.; Leger, J.M.; Yacoubi, N.; Loriers, C. Magnetic properties of some rare earth monoxides LnO (Ln = Pr, Nd, Sm) mixed valence state of SmO. *Sol. State Commun.* **1980**, *33*, 351–353. [CrossRef]
35. Kobayashi, S.; Martín-Cid, A.; Toyoki, K.; Okazaki, H.; Hirosawa, S.; Nakamura, T. Influence of magnetostriction on the lattice constants of the secondary phases in Nd-Fe-B sintered magnets studied by synchrotron X-ray diffraction. *AIP Adv.* **2019**, *9*, 25154. [CrossRef]
36. Eick, H.A.; Baezinger, N.C.; Eyring, L. Lower oxides of samarium and europium. The preparation and crystal structure of $SmO_{0.4\text{-}0.6}$, SmO and EuO. *J. Am. Chem. Soc.* **1956**, *78*, 5147–5149. [CrossRef]
37. Leger, J.M.; Aimonino, P.; Loriers, J.; Dordor, P.; Coqblin, B. Transport properties of SmO. *Phys. Lett. A* **1980**, *80*, 325–327. [CrossRef]
38. Matthias, B.T.; Bozorth, R.M.; Van Vleck, J.H. Ferromagnetic Interaction in EuO. *Phys. Rev. Lett.* **1961**, *7*, 160–161. [CrossRef]
39. Namba, M.; Takatsu, H.; Mikita, R.; Sijia, Y.; Murayama, K.; Li, H.-B.; Terada, R.; Tassel, C.; Ubukata, H.; Ochi, M.; et al. Large perpendicular magnetic anisotropy induced by an intersite charge transfer in strained $EuVO_2H$ films. *J. Am. Chem. Soc.* **2023**, *145*, 21807–21816. [CrossRef]
40. Yamamoto, T.; Kaminaga, K.; Saito, D.; Oka, D.; Fukumura, T. Rock salt structure GdO epitaxial thin film with a high ferromagnetic Curie temperature. *Appl. Phys. Lett.* **2020**, *117*, 052402. [CrossRef]
41. Sasaki, S.; Oka, D.; Kaminaga, K.; Saito, D.; Yamamoto, T.; Abe, N.; Shimizu, H.; Fukumura, T. A high-Tc heavy rare earth monoxide semiconductor TbO with a more than half-filled 4f orbital. *Dalton Trans.* **2022**, *51*, 16648–16652. [CrossRef]
42. Amrillah, T.; Oka, D.; Shimizu, H.; Sasaki, S.; Saito, D.; Kaminaga, K.; Fukumura, T. Rock salt-type HoO epitaxial thin film as a heavy rare-earth monoxide ferromagnetic semiconductor with a Curie temperature above 130 K. *Appl. Phys. Lett.* **2022**, *120*, 082403. [CrossRef]
43. Leger, J.M.; Maugrion, J.; Albert, L.; Achard, J.C.; Lories, C. High pressure synthesis of ytterbium oxides (YbO and Yb_3O_4). *C. R. Acad. Sci. Ser. C Sci. Chim.* **1978**, *286*, 201.
44. Fishel, N.A.; Haschke, J.M.; Eick, H.A. Preparation of ytterbium and europium oxides in liquid ammonia. *Inor. Chem.* **1970**, *9*, 413–414. [CrossRef]
45. Leger, J.M.; Yacoubi, N.; Loriers, J.; McCarthy, G.J.; Rhyne, J.J.; Silber, H.B. (Eds.) *The Rare Earths in Modern Science and Technology*; Plenum Press: New York, NY, USA; London, UK, 1979; Volume 2, p. 203.
46. Zhang, G.X.; Reilly, A.M.; Tkatchenko, A.; Scheffler, M. Performance of various density-functional approximations for cohesive properties of 64 bulk solids. *New J. Phys.* **2018**, *20*, 063020. [CrossRef]
47. Söderlind, P.; Turchi, P.E.A.; Landa, A.; Lordi, V. Ground-state properties of rare-earth metals: An evaluation of density-functional theory. *J. Phys. Cond. Matter* **2014**, *26*, 416001. [CrossRef] [PubMed]
48. Gschneidner, K.A., Jr. Systematics in lanthanide and actinide solids. *J. Alloys Compd.* **1995**, *223*, 165–169. [CrossRef]

49. Horne, M.; Strange, P.; Temmerman, W.M.; Szotek, Z.; Svane, A.; Winter, H. The electronic structure of europium chalcogenides and pnictides. *J. Phys. Cond. Matter* **2004**, *16*, 5061. [CrossRef]
50. Johansson, B. Nature of the electrons in the actinide series. *Phys. Rev. B* **1975**, *11*, 2740. [CrossRef]
51. Kalpana, G.; Palanivel, B.; Rajagopalan, M. Electronic and structural properties of alkaline-earth oxides under high pressure. *Phys. Rev. B* **1995**, *52*, 4–7. [CrossRef] [PubMed]
52. Liu, H.; Mao, H.K.; Somayazulu, M.; Ding, Y.; Meng, Y.; Häusermann, D. B1-to-B2 phase transition of transition-metal monoxide under strong compression. *Phys. Rev. B* **2004**, *70*, 094114. [CrossRef]
53. Sims, C.E.; Barrera, G.D.; Allan, N.L.; Mackrodt, W.C. Thermodynamics and mechanism of the B1-B2 phase transition in group-I halides and group-II oxides. *Phys. Rev. B* **1998**, *57*, 11164. [CrossRef]
54. Richet, P.; Mao, H.K.; Bell, P.M. Static compression and equation of state of CaO to 1.35 Mbar. *J. Geophys. Res.* **1988**, *93*, 15279–15288. [CrossRef]
55. Mao, H.K.; Bell, P.M. Equations of state of MgO and ε Fe under static pressure conditions. *J. Geophys. Res.* **1979**, *84*, 4533–4536. [CrossRef]

Disclaimer/Publisher's Note: The statements, opinions and data contained in all publications are solely those of the individual author(s) and contributor(s) and not of MDPI and/or the editor(s). MDPI and/or the editor(s) disclaim responsibility for any injury to people or property resulting from any ideas, methods, instructions or products referred to in the content.